Journal of Constructional Steel Research 120 (2016) 176–187

Contents lists available at ScienceDirect

Journal of Constructional Steel Research

Cyclic behaviour of Y-shaped eccentrically braced frames fabricated with high-strength steel composite

Feng Wang [a], Mingzhou Su [a,*], Min Hong [b], Yirong Guo [c], Shaohua Li [b]

[a] School of Civil Engineering, Xi'an University of Architecture and Technology, 13 Yanta Road, Xi'an 710055, PR China
[b] Lanzhou Institute of Seismology, China Earthquake Administration, 450 Donggangxi Road, Lanzhou 730000, PR China
[c] College of Electrical and Information Engineering, Lanzhou University of Technology, 287 Langongping Road, Lanzhou 730000, PR China

ARTICLE INFO

Article history:
Received 9 August 2015
Received in revised form 13 December 2015
Accepted 1 January 2016
Available online 14 January 2016

Keywords:
Cyclic test
Seismic performance
High-strength steel (HSS)
Eccentrically braced frame
Vertical link
Y shape

ABSTRACT

Eccentrically braced frames fabricated with high-strength steel (HSS-EBFs) are a new type of seismic structural system. HSS-EBF systems can incorporate Q345 steel (nominal yield strength: 345 MPa) for links, high-strength steel (HSS) (nominal yield strength not less than 460 MPa) for beams and columns, and HSS or Q345 steel for braces. This configuration not only reduces the amount of steel consumed but also increases the usage of HSS in seismic areas. This paper describes an experimental study on HSS-EBFs with vertical links. One half-scale three-storey one-bay by one-bay building with Y-shaped HSS-EBFs (Y-HSS-EBFs) was subjected to a constant vertical linear dead load and cyclic lateral load to examine the seismic performance. The structural failure process, ductility, stiffness, deformation capacity, and energy dissipation capacity of the Y-HSS-EBFs were investigated. The analysis confirmed that the cyclic behaviour of the Y-HSS-EBFs showed good performance for plastic deformation. The force–displacement hysteretic curves of the Y-HSS-EBFs exhibited good plastic deformation behaviour and did not generate the pinching phenomenon. The maximum storey drift ratio and maximum ductility factor on the first storey reached 1/40 and 2.5, respectively. However, severe instability and damage were observed up to the maximum storey drift angle. Plastic deformation is mainly due to the shear deformation of the link web and bending deflection of the link flange at the link-to-beam connection in the first storey. This paper presents an analysis of the experimental investigation and test results can be referred to for the seismic design of this new type of structure.

1. Introduction

Eccentrically braced frames (EBFs) are characterised by both excellent ductility and good energy dissipation. They are widely used as a lateral-force resisting system for multi-storey buildings located in seismic areas [1–3]. The EBF system relies on the plastic deformation of a link beam, and its behaviour with different brace patterns has been investigated [4–9]. Fig. 1 illustrates several common EBF arrangements [10,11]. The eccentricity caused in these frames is represented by the parameter e; the eccentric link is the weakest part of the frame and is the primary dissipation mechanism for the energy resulting from earthquakes [12].

The link is configured either horizontally or vertically. Therefore, there are two general types of EBFs: horizontal (H-EBF) and vertical (V-EBF) [12]. Previous studies [13] have demonstrated that a V-EBF system possesses the advantages of an H-EBF system (e.g. good ductility, high elastic stiffness, and functionality as ductile structural fuses) while also being able to restrict the plastic deformations of the beam members. This arrangement allows links damaged after a massive earthquake to be changed without replacing the beams. Note that, when using vertical links, the section designs of the link beams should be flexible enough to meet the required strength without requiring the uniform cross-section of the beam members [14].

Conventional EBF members often need large cross-sections owing to the use of steel with medium yield strength. This design not only consumes a great deal of steel material but also increases the construction cost. To address this significant drawback, an alternative approach of designing EBFs with HSS (e.g. Q460 or Q690 steel, which have nominal yield strengths f_y of 460 or 690 MPa, respectively) [15] (HSS-EBFs) has been investigated. In these structures, the links use Q345 steel (f_y = 345 MPa), the beams and columns use HSS, and the braces use Q345 steel or HSS [16]. Under earthquake loads, the column, beam, and

Abbreviations: HSS-EBFs, eccentrically braced frames fabricated with high-strength steel; Y-HSS-EBFs, Y-shaped eccentrically braced frames fabricated with high-strength steel; EBFs, eccentrically braced frames; H-EBFs, eccentrically braced frames with horizontal links; V-EBFs, eccentrically braced frames with vertical link; LVDTs, linear variable displacement transducers; HSS, High-strength steel.

* Corresponding author.
E-mail address: sumingzhou@163.com (M. Su).

http://dx.doi.org/10.1016/j.jcsr.2016.01.007
0143-974X/

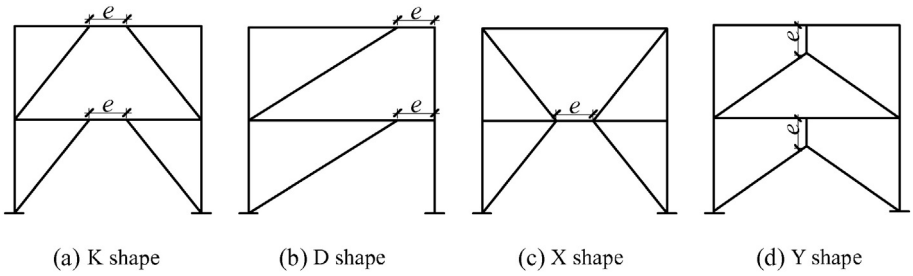

Fig. 1. Typical eccentrically braced frames.

brace members of HSS-EBFs are designed to remain in the elastic stage or show slight plasticity while the links enter the plastic stage completely. This structure can satisfy seismic design requirements with no demands for plastic deformation of the steel used in the column members. Under the same design conditions, HSS-EBFs have smaller member sections than EBFs because of the use of HSS. Because of improvements in the material properties of steel and the further development of steel production processes, HSS has been used in the construction of steel structures around the world, including buildings and bridges. Their advantages include structural safety, architectural functions, economics, and reduced resource consumption [15,17]. Current design specifications such as Eurocode 3 [18] and ANSI/AISC 360-10 [19] extend the scopes up to steel grades of 700 and 690 MPa, respectively [15]. However, the scopes of the Chinese code GB50011-2010 [20] and GB50017-2003 [21] are limited to normal-strength steel structures because HSS has poor plastic deformation capacity. An HSS-EBF structure can satisfy seismic design requirements with little or no demand for plastic deformation of the HSS used in column and beam members. This configuration can increase the usage of HSS in seismic areas. Structural engineers can select the HSS-EBF arrangement for mid-rise buildings because of the low cost [16]. Dubina et al. [22] conducted an experimental study on four K-shaped dual-steel EBF specimens with removable links to examine the seismic behaviour of such systems. Their results showed that these systems can restrict plastic deformations to removable links and decrease the permanent drift of the structure. Duan et al. [23] tested 1:2 scale models of four one-storey and one-bay K-shaped HSS-EBFs under monotonic and cyclic loads. The experimental results suggested that, under cyclic loads, beam–column frames fabricated with HSS remain in the elastic stage while links using conventional steel enter the plastic stage completely. Lian et al. [16] established several finite element models of HSS-EBFs and EBFs to compare the seismic performance and material costs of the two systems. They concluded that HSS-EBFs perform well under strong seismic action and reduce the member sections and structural weight when buildings are less than 16 storeys.

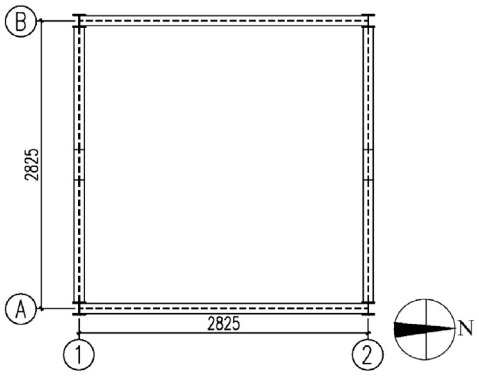

Fig. 2. Plan view of the test specimen.

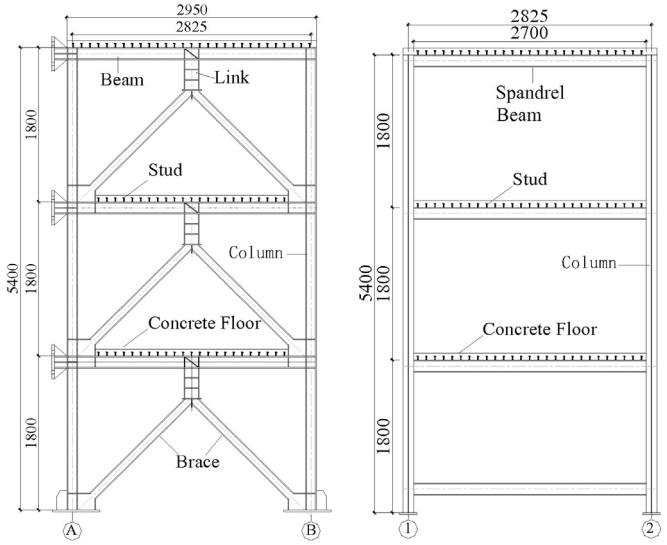

Fig. 3. Elevation view of the test specimen.

These advantages of V-EBFs and HSS-EBFs led the authors to consider a new structural system that combines the two structures: HSS-EBFs with vertical links (V-HSS-EBFs). The Y-shaped V-HSS-EBF (Y-HSS-EBF) is the most common arrangement. Currently, only four one-storey and one-bay planar Y-shaped HSS-EBFs specimens have been statically tested at the Xi'an University of Architecture and Technology in China [24]. Lateral restraints, which can affect the validity and reliability of the test results, were used to avoid out-of-plane instability of the specimens during the experiments. Meanwhile, the seismic response of a multi-storey structure is not similar to that of a single-storey structure. Thus, an additional investigation of multi-storey Y-HSS-EBFs was needed to evaluate the full three-dimensional response. This article presents an experimental study on the seismic performance of one half-scale three-storey (one bay × one bay) steel frame building. The hysteretic behaviour, failure mechanism, and cyclic energy dissipation of the Y-HSS-EBF building were analysed. To the authors' knowledge, this is

Table 1
Sizes of the specimen members.

Member	Section ($h \times b_f \times t_w \times t_f$)
Beam	H140 × 100 × 8 × 10
Spandrel beam	H140 × 100 × 8 × 10
Column	H125 × 125 × 8 × 10
Brace	H100 × 100 × 6 × 10
Link	H180 × 100 × 6 × 10

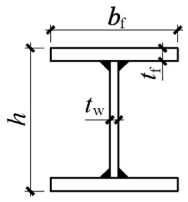

Fig. 4. Specimen sectional dimensions. h: section depth, b_f: flange width, t_w: web thickness, and t_f: flange thickness.

Table 2
Mechanical properties of the steels used.

Steel	Q345B	Q345B	Q460C	Q460C
Thickness t (mm)	6	10	8	10
Yield stress f_y (MPa)	414.70	363.80	473.50	455.60
Ultimate strength f_u (MPa)	542.03	545.80	635.10	598.50
Yield strain ε_y ($\times 10^{-3}$)	1.97	1.81	2.23	2.32
Elastic modulus E ($\times 10^5$ MPa)	2.11	2.01	2.12	1.96
Elongation ratio (%) δ	28.29	28.74	25.36	23.48

the first experimental study on the seismic performance of Y-HSS-EBFs in three dimensions. This paper describes the specimen, loading procedure, test setup, and experimental results. Improvements in the weldability and mechanical properties along with the availability of improved welding processes and welding consumables have allowed HSS to become an economical alternative to conventional steel [16]. The intention of this work was to help spread the use of HSS in building structures in high seismic activity zones.

2. Experimental programme

2.1. Test specimen

The experimental study was conducted at the Xi'an University of Architecture and Technology. In accordance with the relevant Chinese code [20,21], a specimen providing lateral load resistance considered was designed. The design was characterised by a peak ground acceleration of 0.2 g with a 10% probability of exceedance in a 50-year period and a fortification intensity of 8°. The designed frame was located on firm rock (site class II in the Chinese code [20]). Based on the load-bearing capacity of the actuator, one half-scale specimen was designed and fabricated with typical concrete floor decks. Figs. 2 and 3 show the plan and elevation views, respectively, of the test frame. The test structure was a three-storey Y-HSS-EBF building with a one-bay × one-bay plan. The model had a base area of 2.85 m × 2.85 m and storey height of 1.8 m. The test structure was formed by two frames (1, 2) parallel to the loading direction and two frames (A, B) perpendicular to the loading direction. Frames 1 and 2 each had an eccentric bracing system, which are represented by short solid lines in the beam members (see Fig. 2). The length of the link was 350 mm. Table 1 gives the final selection of structural members in the design, where 'H' refers to the welded H-shaped section (see Fig. 4) in units of millimetres. The floor slab thickness was 80 mm, and concrete with a minimum compressive strength of 20.1 MPa was specified. The floor deck of the specimen contained two mats of orthogonal deformed steel bar reinforcements at a spacing of 100 mm. The concrete floor and beams were connected by headed shear studs welded along the middle of the top flange of the beams at intervals of 100 mm (see Fig. 3).

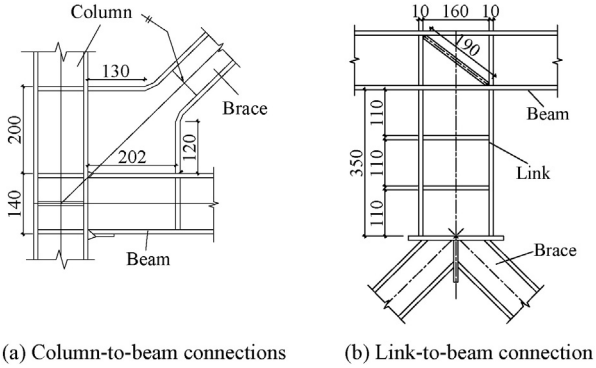

(a) Column-to-beam connections (b) Link-to-beam connection

Fig. 5. Details of connection types.

In the test structure, the columns and beams of the structures used Q460C steel with nominal yield strength of 460 MPa, while the links, braces, and spandrel beams used steel Q345B with a nominal yield strength of 345 MPa. Based on the Chinese code [25], four tensile coupons with different thicknesses and materials were considered in the experiment to determine the material performance of the steel plates used in the specimen. Table 2 gives the results.

Welded joints were used to connect the link to the beam and other elements in the test specimen. Full-depth web stiffeners were fabricated on both sides of the column web and beam web at the column-to-beam connections. The links were also provided with full-depth web stiffeners spaced at 110 mm. Fig. 5 shows schematics of the details for the column-to-beam and link-to-beam connections.

2.2. Test setup and measurement

Fig. 6 illustrates the general arrangement of the experimental setup. The specimen was bolted to six rigid foundation steel grinders, which in turn were restrained by two strong steel beams to prevent the frame specimen from lifting during testing.

Two 1000-kN and one 500-kN servo-actuators were used to apply low-cyclic horizontal loading on the Y-HSS-EBFs through the rigid loading beams. The load proportions of the three load points were maintained at 3:2:1 from top to bottom as determined by the base shear method. Instrumentation including load cells was used to measure the reactions and applied actuator force.

The behaviour of the boundary frames and links during the testing was measured. Fig. 6 shows the measuring instruments. The horizontal displacement of the column-to-beam connections for each storey were measured with six linear variable displacement transducers (LVDTs), and the relative displacement between the frame base and rigid steel beam were measured with two dial gages. To get the principal stresses of the specimen, rosette and uniaxial strain gauges were installed in some higher-stress areas (e.g. link web, link flange, link-to-beam connections, column-to-beam connections, column footing).

2.3. Loading programme

Based on Chinese specifications [26], the vertical loads and horizontal cyclic loads were imposed on the test specimen. First, sand bags were laid on the first floor, second floor, and roof of the specimen to reach dead loads of 6.3, 6.3, and 7.1 kN/m^2, respectively. Then, horizontal loads were applied with mixed force and displacement to the Y-HSS-EBFs in cycles. The loading programme is shown in Fig. 7. In the loading control range, the horizontal cyclic load was incremented at an amplitude of 80 kN, and each increment was applied over one loading cycle. After yielding occurred, the test load was applied by the displacement-control method, and the applied displacement was the roof drift at this moment. In this range, the load incremental amplitude was $0.5\Delta_y$, and three cycles of roof displacements were imposed on the experimental structure for each displacement increment. This process was repeated until either the test load dropped under 85% of the peak

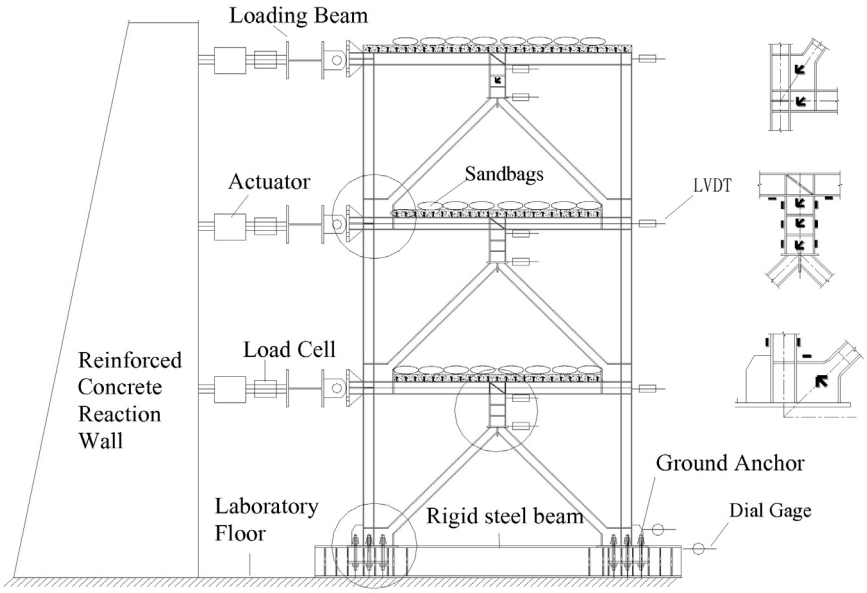

(a) Schematic

(b) Photo

Fig. 6. Test structure and instrumentation (LVDT: linear variable displacement transducer).

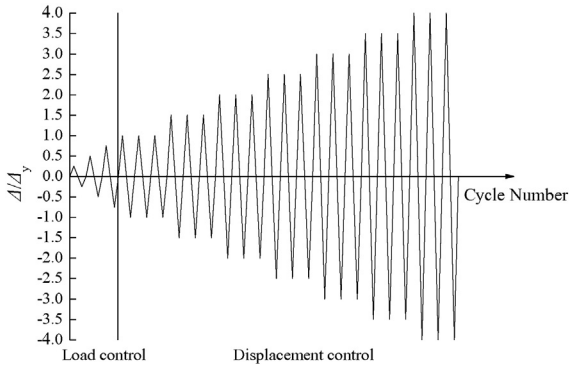

Fig. 7. Loading programme.

load or a significant declination in the loading–displacement loop was observed.

3. Test results and analysis

3.1. Damage evolution and failure mode

The experimental phenomena are summarized as follows. With the force-controlled loading stage, the frame was mostly elastic up to a lateral load of 560 kN. Yielding was observed at the link webs on the first storey at the lateral load of 640 kN. Then, the test load entered displacement-control mode. The test load is a function of the yielding displacement Δ_y, which was measured to be 10.06 mm for the specimen. Fig. 8 shows the structural damage evolution of the specimen under cyclic loading: (1) at the displacement level of $1\Delta_y$, the link webs on the first storey showed ductile yielding (see Fig. 8a); (2) at

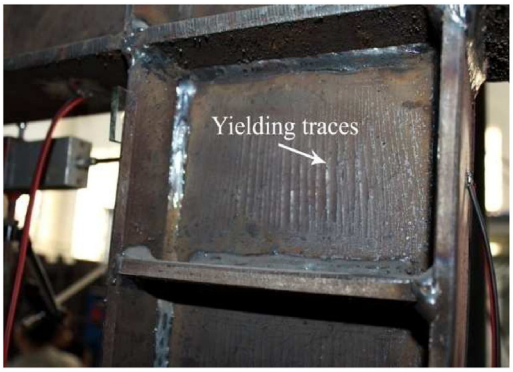

(a) Link web deformation on the first storey

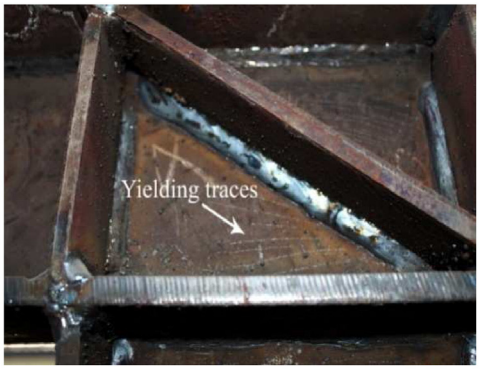

(b) Beam web yielding of the link-to-beam connection on the first storey

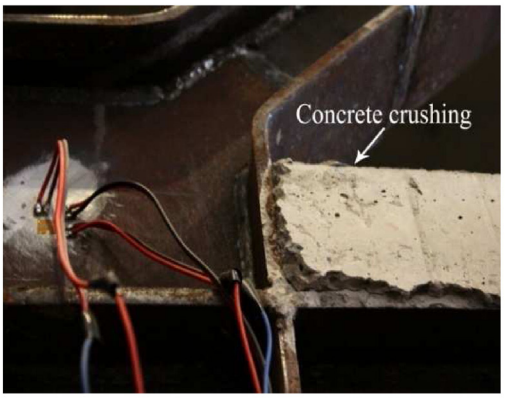

(c) Crushing of the concrete floor on the first storey

(d) Beam stiffener rupture in frame 1 on the first storey

(e) Beam flange fracture in frame 1 on the first storey

(f) Plastic hinge on the first storey

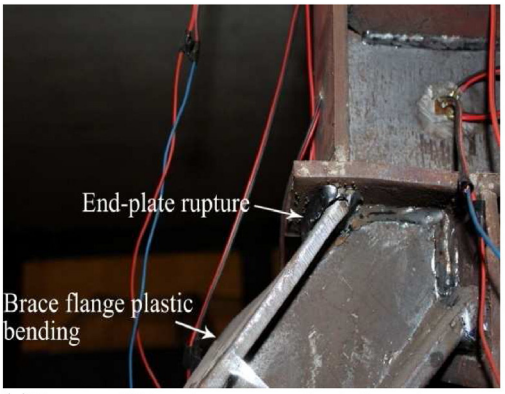

(g) Fracture of link-to-brace connection in frame 1 on the first storey

Fig. 8. Structural damage to the test specimen during the experiment.

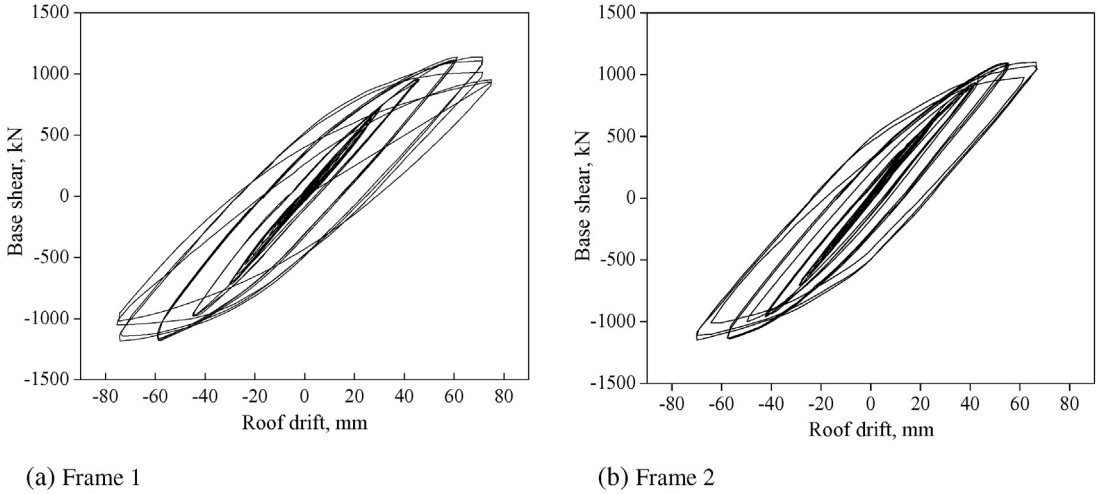

Fig. 9. Force–displacement hysteretic curves.

1.5Δ_y, the link webs on the second storey showed ductile yielding; (3) during the first cycle at 2Δ_y, the beam webs at the link-to-beam connections on the first storey showed partial yielding (see Fig. 8b); (4) during the third cycle at 2Δ_y, the flange at the column B-1 base, the column A-2 base, and the link close to the link-to-beam connection end on the first storey showed ductile yielding, and concrete was crushed on the first floor (see Fig. 8c); (5) during the first cycle at 2.5Δ_y, the beam stiffener in frame 1 on the first storey showed a weld fracture (see Fig. 8d); (6) during the second cycle at 2.5Δ_y, the beam in frame 1 on the first storey showed flange tearing (see Fig. 8e); and (7) during the third cycle at 2.5Δ_y, frame 1 in the first storey started showing out-of-plane displacement (see Fig. 8f). After that, as the beam flange continued to tear, the out-of-plane displacement became increasingly significant, and the corresponding end-plate connecting the link to the diagonal braces fractured (see Fig. 8g). Finally, during the first cycle at 3.0Δ_y, a plastic hinge formed at the link-to-beam connection in frame 1 of the first level and a significant declination of the loading–displacement loop occurred.

3.2. Hysteretic behaviour

Figs. 9 and 10 illustrate the cyclic response and skeleton curves of the base shear force versus roof drift as part of the analysis on the seismic behaviour of the Y-HSS-EBFs.

As shown in Fig. 9, the cyclic response of the Y-HSS-EBFs exhibited good plastic deformation behaviour and did not generate the pinching phenomenon. During the first eight cycles, the specimen showed elastic behaviour, and the hysteretic curves covered a small area. The rigidity of the hysteretic curves degraded slightly on the displacement-controlled stage, and residual displacements occurred upon unloading. The size of the envelope of the hysteretic loops shows no signs of decreasing until the fracture of the link-to-beam connection. The test revealed that the collapse was due to the failure of the link-to-beam connection in frame 1 of the first storey. As illustrated in Fig. 10, the global response curves softened from the peak value; this corresponded to the beam flange crack propagation along the link web in frame 1 on the first storey (see Fig. 8e). With further loading, both plastic bending of the diagonal brace flange and fracture of the corresponding end-plate connecting the link to the diagonal braces occurred (see Fig. 8g).

The most important characteristic of Y-HSS-EBFs is the inequality of the two end moments of the links resulting from the inequality of the stiffness of the floor beam and the bracing members [12], as shown in Fig. 11. The stiffness of the floor beam is much greater than that of braced members. Therefore, the link moment M_1 that developed near the storey beam was larger than the moment M_2 adjacent to the braced members. If the link in frame 1 on the first storey is considered to be a free body, the equilibrium free body diagram is as shown in Fig. 12. The arrangements of the rosette and uniaxial strain gauges on the link

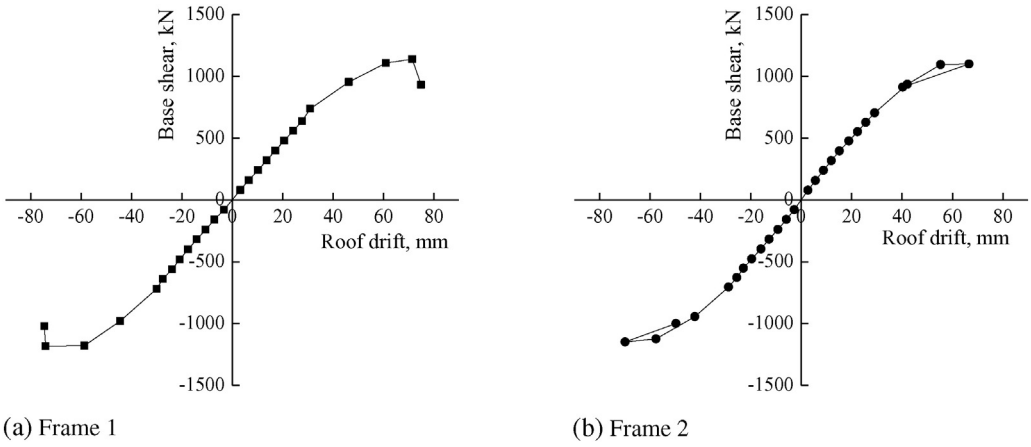

Fig. 10. Skeleton curves of cyclic responses.

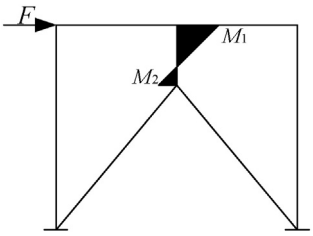

Fig. 11. Bending distribution of Y-HSS-EBFs.

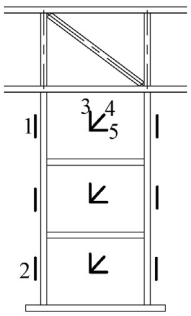

Fig. 13. Link and strain gauges.

web and link flange are shown in Fig. 13. The link moments can be obtained by the material mechanics formulas $\sigma = My / I_z$ and $\sigma = E\varepsilon$ in the elastic range. Therefore, the link moments near the storey beam and adjacent to the braced members can be approximated as $M_A = E_f\varepsilon_1 I_z / y$ and $M_B = -E_f\varepsilon_2 I_z / y$, where E_f is the elastic modulus of the link flange, I_z is the section moment of inertia, y is half of the link height, and ε_1 and ε_2 are the values of uniaxial strain gauges No. 1 and No. 2, respectively. The link shear can be given by the formulas $\tau = (FS) / (I_z d)$ and $\tau = G\gamma$ in the elastic range, and the link shear near the storey beam can be approximated as $F_A = G_w\gamma_A I_z d / S$, where G_w is the shear modulus of the link web, d is the web thickness, S is the static moment of half of the link section, and $\gamma_A = \varepsilon_3 + \varepsilon_5 - 2\varepsilon_4$ is the shear strain of point A. Fig. 14 shows the strain–storey drift skeleton curves. Some of the rosette and uniaxial strain gauges failed during the displacement-control loading stage; thus, only the values of the force-control loading stage are given (see Fig.14). The link moments were proportional to the link flange strain at the corresponding positions, and the differences between ε_1 and ε_2 and between M_A and M_B gradually increased with the lateral load (see Fig. 14). According to the force-balance principle ($\Sigma M = 0$), the link moments and link shear have to satisfy the relationship $M_A + M_B + V_A e_1 = 0$, where $e_1 = 0.25$ m was the distance between the first and third rosette strain gauges along the link. By substituting the values of the strain gauges at the lateral load of 240 kN in the above equations, the relationship $M_A + M_B + V_A e_1 = 10.70 + 1.22 - 46.39 \times 0.25 = 0.32 \approx 0$ was basically satisfied. Towards the end of the force-control loading stage, the uniaxial strain gauge No. 4 reached the yield point strain, and the test load entered the displacement-control stage. This experiment result showed that the combined action of the link flange moment near the storey beam and the large shear load of the link web probably produced the beam flange fracture in frame 1 of the first storey, and the links in the first storey were mainly subjected to shear and flexural failure.

Figs. 15 and 16 show the cyclic responses and skeleton curves for each storey of the specimen; the storey drift is on the horizontal axis, and the storey shear is on the vertical axis. The top storey drift was equal to the displacement of the LVDT on the roof subtracted by the displacement of the LVDT on the middle floor, and the storey shear of the top storey was equal to the actuator force applied to the top loading beam. The second storey drift was equal to the displacement of the LVDT on the middle floor subtracted by the displacement of the LVDT on the bottom floor, and the storey shear of the second storey was equal to the actuator force applied to the top loading beam plus the actuator force applied to the middle loading beam. The first storey drift was equal to the displacement of the LVDT on the bottom floor, and the storey shear of the first storey was equal to the sum of the three applied actuator forces (i.e. the base shear).

As shown in Fig. 15, the first storey demonstrated a relatively stable hysteretic performance and performed well in terms of ductility and energy dissipation. During the loading process, the link webs of the first level yielded first and dissipated a large amount of seismic energy. The link webs of the second level yielded after the first storey and dissipated a small percentage of the seismic energy. There was a linear relationship between the storey shear force and the inter-storey displacement of the third level. Therefore, the stiffness variation was insignificant, and the residual deformation was negligible.

When a displacement of $2.5\Delta_y$ was applied to the specimen, the maximum load-bearing capacity was reached, and the bearing capacity dropped rapidly when the displacement exceeded $2.5\Delta_y$. This degradation was attributed to the observed beam flange fracture of frame 1 on the first storey. Because out-of-plane displacement of frame 1 on the first storey occurred, only the storey drift in frame 1 on the first storey gradually increased with the force degradation, while the other storey drifts showed a clear decrease. Even though the hysteretic loops declined sharply during the first cycle at $3.0\Delta_y$, the specimen still had a surplus bearing capacity after the failure of the link-to-beam connection. This result shows the significance of the redundant bearing capacity provided by the dual seismic resistant system. Later in the experiment, the links and braces severely buckled (see Fig. 8g), and

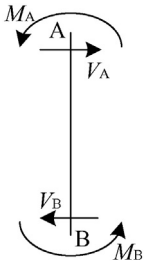

Fig. 12. Free-body diagram of all forces.

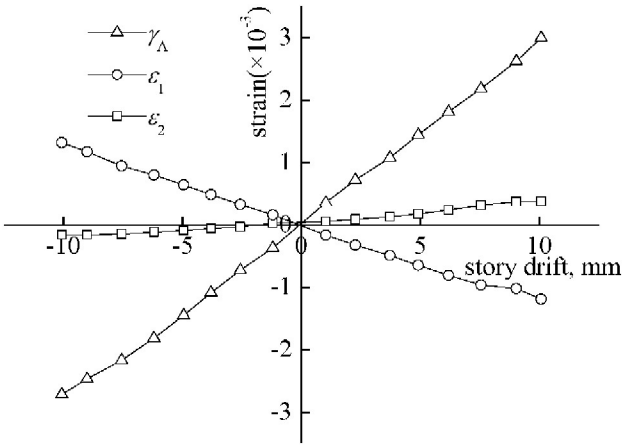

Fig. 14. Strain–storey drift skeleton curves.

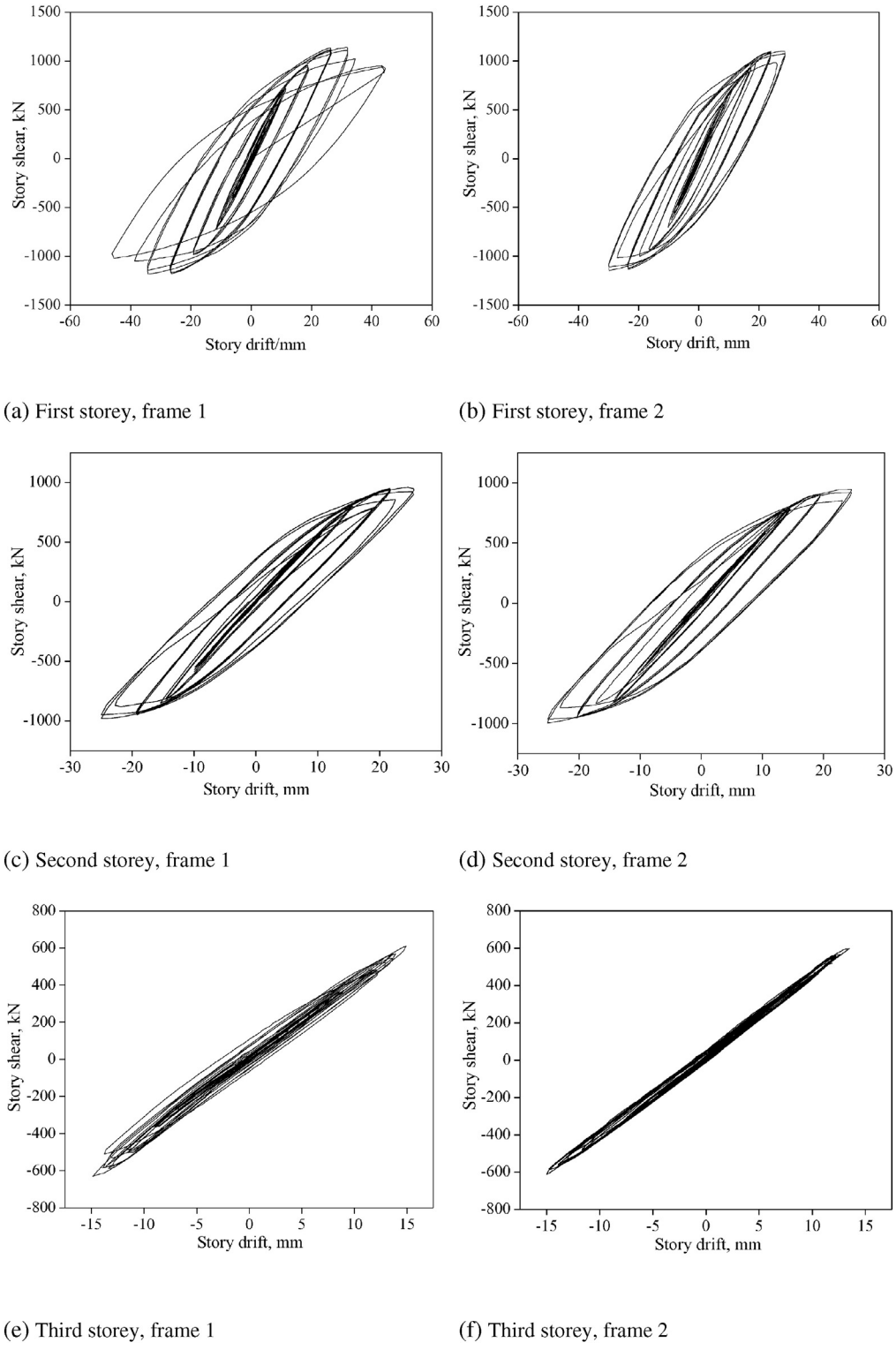

Fig. 15. Storey shear versus storey drift.

the beam–column frames carried most of the lateral load. The Y-HSS-EBFs are typical dual structures and clearly show the importance of providing a reliable energy dissipation mechanism (Y-shaped eccentric brace) within the beam–column frames [27–28]. The HSS-EBFs with vertical links showed good resistance against collapse, and the damaged vertical links can be easily inspected and replaced after a massive earthquake.

3.3. Performance of the test specimen

Table 3 and Table 4 present a related dataset of the three key parameters (i.e. yield point, peak point, and failure point) for analysis of the overall cyclic loading process. The base shear of each frame in the specimen and the corresponding roof drift were given for the three points, as indicated in Table 3, and Table 4 presents the

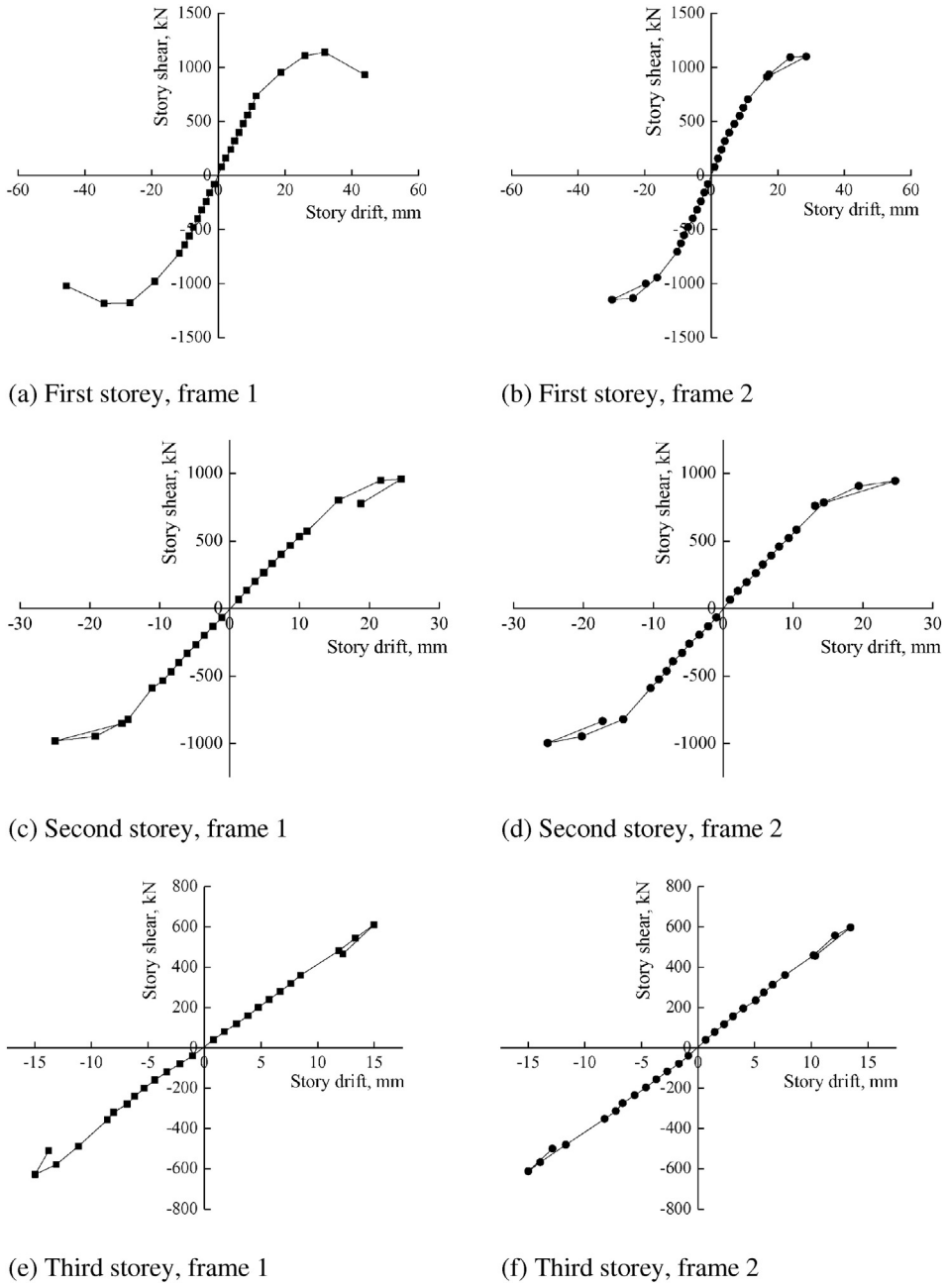

Fig. 16. Skeleton curves for each storey.

storey shear and corresponding storey drift angle for the three points.

The yielding loads of the structures were determined based on the 'equivalent stiffness method' [29], as shown in Fig. 17. Point A is the intersection of the tangent line of the curve through the origin and the horizontal line through peak point C of the skeleton curve. Point B is the intersection of the perpendicular line from point A to the Δ axis and backbone curve. The load corresponding to point B is the yielding

Table 3
Summary of the measured results for the specimen.

Name	Loading direction	Yield point		Peak point		Failure point		P_y/Δ_y/(kN/mm)
		Δ_y/mm	P_y/kN	Δ_p/mm	P_p/kN	Δ_u/mm	P_u/kN	
Frame 1	Positive	49.39	948.35	71.40	1139.02	75.52	968.17	19.20
	Negative	49.93	980.07	74.24	1183.71	74.87	1021.31	19.63
Frame 2	Positive	43.95	908.21	66.60	1100.45	47.65	935.38	20.66
	Negative	46.62	958.02	69.93	1149.19	50.50	999.78	20.55

Table 4
Strength and displacement at different characteristic points of each storey.

Name	Loading direction	Position	Yield point		Peak point		Failure point	
			θ_y/%	V_y/kN	θ_p/%	V_p/kN	θ_u/%	V_u/kN
Frame 1	Positive	First storey	1/101	948.35	1/56	1139.02	1/43	968.17
		Second storey	1/104	839.93	1/73	958.54	1/90	814.76
		Third storey	1/127	578.69	1/120	611.54	1/136	519.81
	Negative	First storey	1/100	980.07	1/53	1183.71	1/40	1021.31
		Second storey	1/103	908.26	1/72	980.93	1/117	851.07
		Third storey	1/125	615.52	1/120	628.16	1/129	533.94
Frame 2	Positive	First storey	1/119	908.21	1/63	1100.45	1/94	935.38
		Second storey	1/107	816.56	1/73	945.61	1/106	803.77
		Third storey	1/149	549.16	1/134	596.76	1/155	507.25
	Negative	First storey	1/111	958.02	1/60	1149.19	1/91	999.78
		Second storey	1/103	896.33	1/72	996.33	1/103	846.88
		Third storey	1/140	550.12	1/120	612.15	1/136	520.33

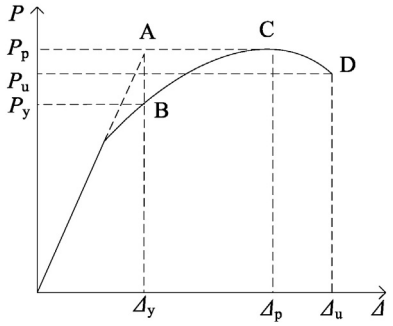

Fig. 17. Schematic diagram of equivalent stiffness method.

Table 5
Cyclic energy dissipation of the specimen.

Name	Displacement	Global structure		First-storey		Second-storey		Third-storey	
		E/kJ	C_e	E/kJ	C_e	E/kJ	C_e	E/kJ	C_e
Frame 1	$1.0\Delta_y$	4.36	0.19	2.75	0.31	0.46	0.06	0.36	0.13
	$1.5\Delta_y$	17.69	0.38	13.84	0.75	2.89	0.25	1.51	0.25
	$2.0\Delta_y$	56.25	0.82	36.66	1.19	13.48	0.69	1.65	0.19
	$2.5\Delta_y$	96.54	1.19	56.91	1.57	25.11	1.07	2.98	0.44
	$3.0\Delta_y$	83.96	1.13	66.39	1.51	8.73	0.63	2.31	0.38
Frame 2	$1.0\Delta_y$	3.22	0.19	1.80	0.25	0.45	0.06	0.24	0.06
	$1.5\Delta_y$	14.21	0.38	9.85	0.63	2.38	0.19	0.68	0.13
	$2.0\Delta_y$	46.68	0.75	28.91	1.07	13.32	0.75	1.21	0.19
	$2.5\Delta_y$	84.02	1.13	44.12	1.38	23.56	1.01	1.24	0.13
	$3.0\Delta_y$	23.11	0.57	15.67	0.88	4.61	0.38	0.68	0.13

load P_y, the load corresponding to peak point C is the maximum load. The displacement corresponding to point B is the yielding displacement Δ_y, and the displacement corresponding to point C is the peak displacement Δ_p. Point D on the skeleton curve corresponds to 85% of the maximum load (or the ultimate load with the skeleton curve not achieving 85% of the maximum load at the end of the experiment), and the displacement corresponding to point D is the ultimate displacement Δ_u. The ratio of the ultimate displacement Δ_u and yielding displacement Δ_y is the ductility of the structure.

As summarized in Table 3, the following data were collected and analysed: (1) P_y, P_p, and P_u = the yielding load, peak load, and ultimate load, respectively; (2) Δ_y, Δ_p, and Δ_u = the displacements of the roof corresponding to the loads P_y, P_p, and P_u, respectively; and (3) P_y/Δ_y = lateral elastic frame stiffness before link buckling.

Table 4 gives the experimental results of each storey corresponding to the loads P_y, P_p, and P_u, respectively: V_y, V_p, and V_u are the storey shear and θ_y, θ_p, and θ_f, are the storey drift ratio. The storey drift ratio is defined as $\theta_i = \Delta_i / H$, where Δ_i is the storey drift and H is the storey height.

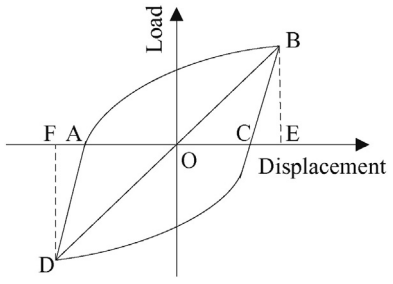

Fig. 18. Calculation of the energy dissipation coefficient.

Table 3 indicates that the base shear and roof drift in the positive and negative directions of the test specimen were approximately the same, and the specimen had high strength and elastic stiffness. The combined effect of both the beam–column frame and eccentric brace system contributed to the lateral stiffness of the Y-HSS-EBFs. The beam–column frame fabricated with HSS can be considered to be a reserve defence for earthquake resistance apart from the bracing system. This paper provides the typical characteristics of a Y-HSS-EBF structure under a cyclic load. The response can be summed up with three effects: cumulative damage to the vertical links, surplus bearing capacity contributed by the beam–column frame fabricated with HSS, and little or no nonlinear deformations in the beam members. At the displacement level of $2.0\Delta_y$, ductile yielding of the link webs, link flanges, and beam webs on the first storey and ductile yielding of the column bases occurred. These results are in line with the typical characteristics of a Y-HSS-EBF structure under a cyclic load. Table 3 also indicates that frame 1 endured a larger lateral force than frame 2 because of the initial geometric imperfections from fabrication and assembly. At the displacement level of $2.5\Delta_y$, weld fracture of the beam stiffener and beam flange tearing occurred. These unwanted behaviours resulted from the loading setup. Owing to the influence of the initial imperfection of the structure, there were some minor differences in the lateral stiffness between the two frames. When the test entered into the elastoplastic phase, the unwanted behaviour due to differences in the displacement and horizontal load distribution of the loading beam ends gradually occurred. The test was stopped after the completion of the displacement $3.0\Delta_y$. However, some strength and ductility contributed by the beam–column frame remained.

As indicated in Table 4, the maximum storey drift ratio of the test specimen was 1/40, which is much greater than the limit value specified by the Chinese Seismic Design Code (GB50011-2010) [20], where the limit is 1/50. This indicates that the test specimen had good elastoplastic deformation capacity. The start of yielding was clearly observed when the storey drift angle reaches 1/101 for frame 1 and 1/119 for frame 2 on the first storey (see Table 4). The links on the first storey accessed the elastoplastic deformation phase, and permanent deformation occurred. At the beginning of the test, the inter-storey drift of frame 1 was nearly the same as that of frame 2 on the first storey. However, during the final two cycles of the load process, frame 1 on the first storey began to absorb more of the total structure deformation as a result of the out-of-plane displacement. The maximum ductility factors of frame 1 on the first storey reached 2.5, and the specimen generally had good ductility. The maximum plastic rotation of the link from the test was 0.08 rad, which reached the implied minimum value outlined in the seismic design provisions for EBFs [30]. Only one link in frame 1 on the first storey reached this limit. There are two reasons for this: first, frame 1 initially failed because the horizontal load distribution was asymmetric between the two frames; second, the first level with the maximal link rotation angle endured the largest lateral force.

3.4. Cyclic energy dissipation

The energy dissipation coefficient C_e, which can be calculated by dividing the sum of the areas S_{ABC} and S_{CDA} by the sum of the areas S_{OBE} and S_{ODF} (see Fig. 18), was introduced and used as an index to evaluate the dissipative capacity of the vertical links in Y-HSS-EBFs under a seismic load.

The energy dissipation coefficient increased steadily after the links began to yield, which indicates that the dissipated energies gradually increased as the displacement increased. During the test, the links on the first storey dissipated a large amount of energy, and the links on the second storey demonstrated limited energy dissipation capacity during the subsequent cycles. However, the third level of the specimen remained in the elastic state with no plastic deformation. Table 5 summarizes the values for the energy dissipation coefficient C_e and dissipated energy value E, which represent the energy dissipation capacity of the test structure. The dissipated energies increased steadily after the frame members began to yield, and more than 50% cyclic energy was dissipated by the first storey. The maximum values of the energy dissipation coefficients of the two frames on the first storey both exceeded 1.3, which indicates that the Y-HSS-EBF structure had excellent energy dissipation capacity.

4. Conclusions

This paper presents an experimental study on a half-scale test model. In this test programme, a three-storey one-bay by one-bay building with Y-HSS-EBFs was loaded cyclically to failure. Based on the test data and analyses, the major conclusions are as follows:

1. The failure process of the specimen under reversed cyclic loading included ductile yielding of the link webs, link flanges, and beam webs on the first storey; ductile yielding of the link webs on the second storey; ductile yielding of the column bases; concrete crushing on the first floor; and weld fracture of the beam stiffener, beam flange tearing, and out-of-plane displacement of frame 1 on the first storey. The final failure of the specimen occurred by plastic hinges formed at the link-to-beam connections in frame 1 of the first storey.
2. The yielding pattern of the specimen indicated that the links in the first storey were subjected to shear and flexural yielding, and the link moment that developed near the storey beam was greater than the moment adjacent to the braced members.
3. The cyclic response of the specimen exhibited plastic deformability and did not generate the pinch phenomenon. The hysteretic curves of the storey shear versus the storey drift indicated that a larger plastic deformation occurred on the first storey, and minor or no plastic deformation occurred on the second or third levels.
4. Y-HSS-EBFs possess high elastic stiffness, good deformability, and excellent energy dissipation capacity. The maximum storey drift ratio of frame 1 on the first storey was larger than 1/50, and the first storey dissipated more than 50% of the cyclic energy.
5. After the link-to-beam connection failure, some strength and ductility remained from the beam–column frame fabricated with HSS. The damaged links in Y-HSS-EBFs can be quickly inspected and replaced.

Acknowledgements

The authors are grateful for the financial support from the National Natural Science Foundation of China (Grant No. 51178382). The authors also thank the Xi'an University of Architecture and Technology staff and students for their kindest help in ensuring the success of this experiment.

References

[1] T. Okazaki, M.D. Engelhardt, Cyclic loading behavior of EBF links constructed of ASTM A992 steel, J. Constr. Steel Res. 63 (2007) 751–765.
[2] G.S. Prinz, P.W. Richards, Eccentrically braced frame links with reduced web sections, J. Constr. Steel Res. 65 (2009) 1971–1978.
[3] C.K. Gulec, B. Gibbons, A. Chen, A.S. Whittaker, Damage states and fragility functions for link beams in eccentrically braced frames, J. Constr. Steel Res. 67 (2011) 1299–1309.
[4] K.D. Hjelmstad, E.P. Popov, Characteristics of eccentrically braced frames, J. Struct. Eng. 110 (1984) 340–353.
[5] J.O. Malley, E.P. Popov, Shear links in eccentrically braced frames, J. Struct. Eng. 110 (1984) 2275–2295.
[6] K. Kasai, E.P. Popov, General behavior of WF steel shear link beams, J. Struct. Eng. 112 (1986) 362–382.
[7] D. Özhendekci, N. Özhendekci, Effects of the frame geometry on the weight and inelastic behaviour of eccentrically braced chevron steel frames, J. Constr. Steel Res. 64 (2008) 326–343.
[8] K.D. Hjelmstad, S.G. Lee, Lateral buckling of beams in eccentrically-braced frames, J. Constr. Steel Res. 14 (1989) 251–272.
[9] J.W. Berman, M. Bruneau, Experimental and analytical investigation of tubular links for eccentrically braced frames, Eng. Struct. 29 (2007) 1929–1938.
[10] K.D. Hjelmstad, E.P. Popov, Cyclic behavior and design of link beams, J. Struct. Eng. 109 (1983) 2387–2403.
[11] A. Ghobarah, E.H. Abou, Rehabilitation of a reinforced concrete frame using eccentric steel, Eng. Struct. 23 (2001) 745–755.
[12] M.A. Shayanfar, M.A. Barkhordari, A.R. Rezaeian, Experimental study of cyclic behavior of composite vertical shear link in eccentrically braced frames, Steel Compos. Struct. 12 (2011) 13–29.
[13] M.A. Shayanfar, A.R. Rezaeian, A. Zanganeh, Seismic performance of eccentrically braced frame with vertical link using PBPD method, Struct. Des. Tall Special Build. 23 (2012) 1–21.
[14] N. Mansour, C. Christopoulos, R. Tremblay, Experimental validation of replaceable shear links for eccentrically braced steel frames, J. Struct. Eng. ASCE 137 (2011) 1141–1152.
[15] G. Shi, W.J. Zhou, Y. Bai, C.C. Lin, Local buckling of 460 MPa high strength steel welded section stub columns under axial compression, J. Constr. Steel Res. 100 (2014) 60–70.
[16] M. Lian, M.Z. Su, Y. Guo, Seismic performance of eccentrically braced frames with high strength steel combination, Steel Compos. Struct. 18 (2015) 1517–1539.
[17] H.Y. Ban, G. Shi, Y.J. Shi, Y.Q. Wang, Overall buckling behavior of 460 MPa high strength steel columns: experimental investigation and design method, J. Constr. Steel Res. 74 (4) (2012) 140–150.
[18] BS EN 1993-1-12, Eurocode 3: Design of Steel Structures: Part 1–12: Additional Rules for the Extension of EN 1993 up to Steel Grades S700, BSI, London, 2007.
[19] ANSI/AISC 360–05, Specification for Structural Steel Buildings, AISC, INC, Chicago, 2005.
[20] GB50011-2010, Code for Seismic Design of Buildings, Architecture Industrial Press of China, Beijing, 2010 (in Chinese).
[21] GB 50017-2003, Code for Design of Steel Structures, China Architecture &Building Press, Beijing, 2006 (in Chinese).
[22] D. Dubina, A. Stratan, F. Dinu, Dual high-strength steel eccentrically braced frames with removable links, Earthq. Eng. Struct. Dyn. 37 (2008) 1703–1720.
[23] L.S. Duan, M.Z. Su, Q.L. Hao, P.P. Jiao, Experimental study on seismic behavior of high-strength steel composite K-type eccentrically braced frames, J. Build. Struct. 35 (2014) 15–28 (in Chinese).
[24] L.S. Duan, M.Z. Su, P.-P. Jiao, Q.L. Hao, Experimental study on seismic behavior of high-strength steel composite Y-type eccentrically braced frames, J. Build. Struct. 35 (2014) 89–96 (in Chinese).
[25] GB/T228, Metallic Materials—Tensile Testing at Ambient Temperature, Chinese Standard Press, Beijing, 2002 (in Chinese).
[26] JGJ 101-1996, Specification of Testing Methods for Earthquake Resistant Building, China Architecture & Building Press, Beijing, 1997 (in Chinese).

[27] D.A. Foutch, S.C. Goel, C.W. Roeder, Seismic testing of full-scale steel building—part I, J. Struct. Eng. ASCE 113 (1987) 2111–2129.
[28] C.W. Roeder, D.A. Foutch, S.C. Goel, Seismic testing of full-scale steel building—part II, J. Struct. Eng. ASCE 113 (1987) 2130–2145.
[29] R. Park, Ductility evaluation from laboratory and analytical testing, Proceedings of 9th World Conference on Earthquake Engineering, Tokyo, Japan 1988, pp. 605–616.
[30] AISC, Seismic Provisions for Structural Steel Buildings, ANSI/AISC 341–10, American Institute of Steel Construction, Chicago, IL, 2010.